Investigation of non-covalent interactions in mixed clusters of heterocyclic aromatic compounds: A supersonic jet study combined with quantum chemistry calculations

A Thesis Submitted Towards Partial Fulfillment of

BS-MS Dual Degree Programme

by

Vedant Pande

Under the Guidance of

Dr. Aloke Das

Assistant Professor

Department of Chemistry

IISER Pune

Department of Chemistry

Indian Institute of Science Education and Research Pune

Certificate

This is to certify that this dissertation entitled "Investigation of non-covalent interactions in mixed clusters of heterocyclic aromatic compounds: A supersonic jet study combined with quantum chemistry calculations" towards the partial fulfillment of the BS-MS dual degree programme at the Indian Institute of Science Education and Research, Pune, represents original research carried out by Vedant Pande at IISER Pune under the supervision of Dr. Aloke Das during the academic year 2010-2011.

Name and signature of the student

Supervisor	**Head (Chemical Sciences)**
Date:	**Date:**
Place:	**Place:**

ACKNOWLEDGEMENTS

Foremost, I would like to express my sincere and deepest gratitude to my advisor Dr. Aloke Das whose personal guidance, support and encouragement throughout my project enable me to write this thesis.

It is a pleasure to thank my fellow lab mates Sumit Kumar, Indu Kaul and Partha Biswas for their valuable suggestions and encouragements.

I also acknowledge my classmates Ashutosh, Hemant, Prakhar, Rakesh, Subhajit, Vivek for making this period joyful.

Last but not the least, I would like thank my family for their consistent unconditional support and inspiring me to achieve new levels of success.

Vedant Pande

TABLE OF CONTENTS

Dedicated to my parents

Chapter 1

Introduction

1.1. Importance of non-covalent interactions

Non-covalent interactions are weak in nature but collectively these interactions are proved to be quite strong and are crucial to specific structures of bio-molecules.[1-2] These weak interactions also play a central role in crystal structures, self-assembly, molecular recognition, DNA intercalation etc.[3-6] The function of the biomolecules depends very much on their specific shapes which are governed by various non-covalent interactions only. Double helical structure of DNA, various folded structures of proteins are some of the examples of specific structures of the biomolecules. It could be thought that life probably would not exist in absence of these weak intermolecular interactions. Due to this enormous significance of non-bonding interactions in life, material science, drug discovery etc., there has been tremendous interest to understand these interactions in details by using various experimental as well as theoretical methods. The experiments to determine the non-covalent interactions have been performed in both solution and isolated gas phase (i.e. supersonic jet) quite extensively. But it is always preferable to study these weak interactions in isolated gas phase, where additional intermolecular interactions due to bulk solvent as well as interactions among molecular systems under study are absent. The data obtained in the supersonic jet are also very much suitable to compare with the results from high level quantum chemistry calculations. Thus studies in the supersonic jet combined with quantum chemistry calculations provide quantitative information about the intermolecular interactions present in molecular systems as well as clusters.

1.2. Classification of non-covalent interactions

Non-covalent interactions in clusters are primarily classified into two different categories namely hydrogen bonding and dispersion interactions.

1.2.1. Hydrogen bonding interaction

The Hydrogen bond is a crucial phenomenon in structural biology especially because its ability to control the structures and the directionality of the bond. The simplest definition of a hydrogen bond is an attractive interaction of a hydrogen atom with an electronegative atom. Generally the hydrogen atom is connected to another electronegative atom through a covalent bond. Pauling first introduced the concept of hydrogen bond in his book "*The nature of Chemical bond*".[7] Since then extensive research has been done on the attributes of the hydrogen bond. Pauling's work also highlighted the electrostatic nature of the hydrogen bond and stated that in a X-H…A system, the elements X and A should be electronegative. The definition of hydrogen bond was further refined till Pimental and McClellan(1960) claimed that hydrogen bonding is possible irrespective of electronegative nature of A and X.[8] The study of hydrogen bonding with groups like C-H and π-acceptors has become an interesting area of research. Later Steiner and Saenger stated that A can have a partial or full negative charge, H carries a positive charge and charge on X is more negative than H.[9] Thus, there are two types of hydrogen bonds; (i) Strong hydrogen bond, where both X and A are electronegative atoms (O, N). Electrostatic interactions representing dipole-dipole or a dipole-charge interaction with the relevant charges being around the atomic nuclei are dominant in strong hydrogen bonding. Here weak sharing of an electron pair between hydrogen atom and an electronegative atom takes place. This is a contact-like interaction in which the bonding depends on orbital overlap. The energy range of strong hydrogen bonds is 4-15 kcal/mol. (ii) Weak hydrogen bond, where X is carbon atom and Y is electronegative atom (i.e. C-H…N, C-H…O etc). Weak hydrogen bonding is an interaction between a hydrogen atom in a system X-H…A in which one or even both structural moieties have moderate or low electronegativity. Nature of donor and acceptor group plays a substantial role in weak hydrogen bonds. The bond energy is less than 4 kcal/mol in case of weak hydrogen bonding. It has been reported recently that sulphur also makes quite strong hydrogen bond. Although fluorine (F) is the strongest electronegative atom, it is a very weak hydrogen bond acceptor as its proton affinity is very low. Most biological reactions occur at room temperature, in very short time spans. In terms of strength, the hydrogen bond lies in between covalent and van der Waals interaction and thus, the energy range of hydrogen bonding allows these bonds to associate and dissociate quickly at ambient temperature. The simplest example of a hydrogen bond is found in water molecules.

1.2.2. Dispersion interaction

Dispersion interactions are due to transient, random charges that are continuously generated all over the molecule. Apart from polar and ionic interactions, it is the third type of interactive mechanism that allows molecules to exert force on one another. This is a part of van der Waals forces and mainly dominates the interaction of non-polar molecules. Due to the fluctuations in the instantaneous position of electrons these non-polar molecules posses transient dipoles. The attraction between two instantaneous dipoles give rise to an induced-dipole-induced-dipole interaction. The strength of the dispersion interaction depends on the polarizability of both the molecules. Quantum mechanical theory is used to explain this interaction by using the second order perturbation theory in which the interaction energy expression contains a sum over states. In this theory the first order perturbation represents the columbic interaction between electrons and nuclei of the two monomers forming a dimer. The final expression for the interaction energy (V) is given in equation 1.1 which is also known as the London formula, where α'_1 and α'_2 are the dipole polarizabilities of the respective atoms, I_1 and I_2 are the first ionization potentials of the atoms and r is the intermolecular distance.

$$V = -\frac{C}{r^6} \qquad c = \frac{2}{3}\alpha'_1\alpha'_2 \frac{I_1 I_2}{I_1 + I_2} \tag{1.1}$$

Dispersion interactions can be classified in two types namely, π-hydrogen bonding and π-π stacking interactions. Electron-rich systems like aromatic rings constitute the class of the non-conventional acceptors. In these interactions, the donor interacts with electrons in a π orbital of a multiple bond (negative charge of the π cloud) and hence is a dipole-quadrupole kind of interaction. These are known as π-hydrogen bonds (non-conventional hydrogen bonds such as C-H…π, N-H…π, etc). Acetylene dimer is a very good example of C-H…π hydrogen bonding.[10] The stability of these systems is due to dispersion interaction with electrostatic terms being a moderate component. π-π interactions generally occur due to stacked arrangement of aromatic molecules. Presence of π-orbitals, which act as one of the source for such molecular interactions, is the reason for the name *π-π interaction*. Dispersive forces mainly dominate the origin of this interaction. It is believed that weak electrostatic, induced dipole and dispersion are the possible contributors to stacking. The distance between the two π faces is around 3.5 Å. Stacking occurs through π-π interactions in vertical plane which plays an important role in molecular clusters.

The most common example of stacked system is stacking of consecutive base-pairs in DNA which adds to its stability and overlap of non-polar rings in proteins. The most studied system in the literature is the benzene dimer which is model for π-π interaction.

1.3. Non-covalent interactions in biological structures and supramolecular chemistry

1.3.1. Biological structures

The physiological and biological properties of biomolecules are largely related to their specific shape which in turn is governed by non-covalent interactions. The role of non-covalent interactions in determining the specificity of the structures of three major macromolecules that are essential for all forms of life: DNA, RNA and proteins, is discussed below.

Hydrogen bonding between the base pairs is the main reason for its double helical structure of DNA. The stabilization of this structure is primarily due to two forces – Hydrogen bonding which happens between the nucleotides and base-stacking interactions which happen among the aromatic bases. Nitrogenous bases in nucleotides are made up of aromatic purines and pyrimidines, the faces of these aromatic rings (as these rings are almost perpendicular to the strands) participate in aromatic interaction. Aromatic interaction makes the pi-bonds to overlap with the pi-bonds of adjacent bases. This interaction within the double-stranded DNA stabilizes the structure. The phenomenon of base pairing best exemplifies the importance of the non-covalent interactions; the base on one strand forms hydrogen bond with a specific type of base on the other strand. This is known as complementary base pairing, where purines form hydrogen bonds with pyrimidines with the specificity that adenine binds only to thymine and guanine to cytosine. As discussed earlier the energy range of hydrogen bonds allows association and dissociation easily. This complementary bonding helps the information on the double-stranded sequence to be duplicated on each strand. Adenine and thymine form two hydrogen bonds whereas guanine and thymine form three hydrogen bonds. The additional hydrogen bond between G & C gives more stability and hence DNA with high GC content is more stable. Another example of non-covalent interaction in DNA is the formation of G-quadruplex structure. This structure is stabilized mainly by hydrogen bonding between the edges of the bases.

The functional form of single stranded RNA require specific structural form which is attained through hydrogen bonds within the molecule. This leads to different domains of the

secondary structure like bulges and internal loops. In translation the transfer RNA binds to a specific sequence of messenger RNA through hydrogen bonding. Stacking interactions, which are energetically favorable, are observed in nucleic acid bases in water help in stabilizing the secondary and tertiary structure of DNA and RNA.

There are four different aspects of protein structure, primary, secondary, tertiary and quaternary. In the secondary structure of proteins, alpha-helix, beta-sheets and turns, the repeating local structures, are stabilized through hydrogen bonds. The tertiary structure is also stabilized by hydrogen bonds in combination with the formation of a hydrophobic core, disulfide bonds, etc. The quaternary structure is held together by ionic, hydrogen and disulfide bonds between amino acids of different peptides. Dehydrons are an example where intramolecular hydrogen bonds are present within proteins. Aromatic stacking is also observed in proteins where two relatively non-polar rings overlap.

DNA intercalation is insertion between two successive DNA base pairs. Water and cations bind to specific DNA sequences through non-covalent interactions. It is important to study the participation of water molecules in ligand-DNA interactions which involves hydrogen bonding as the main interaction. Drug molecules also intercalate into DNA and the study of the mechanism indicates that complicated binding occurs through non-covalent interactions.

1.3.2. Supramolecular chemistry

Supramolecular chemistry deals with the assembly of large number of molecules held together by short, medium and long-range interaction. There is a higher degree of order in a crystal structure which is made up of ordered supramolecular systems. Non-covalent interactions are reported to be important in these crystal structures. Keegstra *et al*. (1994) demonstrated the layer structure in 2-methoxy-1,4-benzoquinone in which extensive involvement of short C-H…O bonds were found.[11] There are many other studies in which nitro compounds were shown to have C-H…X hydrogen bonds which determine their crystal packing. F.D. Lewis *et al*. (1996) discussed the interplay between N-H…O, C-H…O and π-π interactions in secondary arenedicarboxamides. [12]

1.4. Previous studies

Solution and gas phase experiments have been widely used for investigation of non-covalent interactions. The classical method for studying such interactions in solution phase is vibrational spectroscopy. Intramolecular O-H…π bonds were investigated by studying the IR absorption spectra of ortho-substituted phenols in dilute CCl_4 solutions.[13] The strong red shift of the O-H stretching vibration indicates the formation of hydrogen bonds. Intermolecular hydrogen bonds have been studied using 2-D IR spectroscopy.[14] Investigation of complexes of 2,6-dimethyl pyridine with water show co-operative participation of non-covalent interactions and this determines the properties of the system.[15] This technique proves to be useful in studying strong hydrogen bonds but for non-conventional hydrogen bonding, aromatic π-π interactions, the results are not very clear as the equilibrium geometry is not directly observed in condensed phase.

Non-covalently bonded aromatic dimers have been studied extensively using laser spectroscopic techniques in the gas phase experimentally as well as theoretically. Experimental evidence of hydrogen bonded systems X-H…A, where X and A both are electronegative are many in the literature. The study of intermolecular hydrogen bonding in aromatic clusters like benzene…$(H_2O)_n$,[16] phenol…$(H_2O)_n$,[17] phenol-$(ammonia)_n$,[18] are the examples where strong hydrogen bonding occurs as both X and A in these systems are electronegative. It is interesting to note that the role of OH group of phenol in the phenol…$(water)_n$ cluster can be proton accepting or donating, but experimentally only the proton donating OH is observed. Aniline is the simplest amine with an aromatic ring and shows both NH-σ and NH-π type of hydrogen bonding. NH-σ is the type in which hydrogen bonding is between NH group and the lone pair of electronegative atom of another molecule. Many complexes of aniline have been investigated in the gas phase.[19-20] Nakanga and Ito studied the hydrogen bond interaction in aniline-furan complex in which comparison between the neutral complex and the cation is discussed.[21] Indole which is the main chromophore of tryptophan is found to be proton-donating when clusters of indole with water, alcohols, amines and other aromatic molecules is studied in the supersonic jets. Hager *et al*. have the discussed about the shifts of the band origins of these complexes and the relative strength of the hydrogen bond.[22] Non-conventional hydrogen bonding like NH-π and CH-π have also been investigated in gas phase. Benzene dimer is the most extensively studied

system and the results show that the most stable structure is the T-shaped with CH-π interaction.[23] Interaction energies of C_2H_4…CH_4 and C_2H_6…CH_4 dimers using high-level ab–initio calculations shows the comparison between electrostatic and dispersion interaction and proves to be a model for CH-π interaction.[24] In 1959 Oki and Imamura first reported the NH-π while studying *N*-benzylaniline and its derivatives by the measurement of their IR spectra.[25] Since then many systems are reported which show this type of non-conventional hydrogen-bonding.[26] Perutz *et al*. reported the NH-π interaction in the hemoglobin-drug complex.[27] Benzene-ammonia complex has been extensively studied both experimentally and theoretically.[28] As a model for NH-π interaction 2-pyridone-benzene complex was studied using laser spectroscopy where the interaction was comparable to the intermediate-strength hydrogen bonds.[29] Recently, SH…π hydrogen-bonded complexes of H_2S with indole and 3-methylindole were reported by Biswal *et al*. The comparison of this π-hydrogen bond with the other type CH…π, NH…π suggest that SH…π is the strongest among them.[30]

Apart from hydrogen bonding, π-π interactions are also ubiquitous in aromatic mixed dimers. Theoretical study of benzene dimer suggests that both T-shaped and parallel-displaced geometries are almost isoenergetic. In gas phase, however, only the T-shaped conformer exists. Many theoretical reports present π-stacked conformers in N-heteroaromatic systems. Mishra *et al.* discussed the stacking and spreading interactions in pyridine dimer and trimer systems.[31] The optimized and the binding energy values for different conformers is reported to compare the two interactions. Laser spectroscopy of phenylacetylene and 1,3,5-triazine suggest that 1,3,5-triazine primarily interacts with the π-electron density of acetylene ring of phenylacetylene. Ab-initio calculations suggest the formation of a displaced π-π structure.[32] The experimental evidence of π-stacked dimers in gas phase is very rare though there are many theoretical studies reported in the literature.

1.5. Motivation behind present study

Gas phase laser spectroscopy in a supersonic jet combined with high level quantum chemistry calculations provide an useful means to study non-covalently bonded aromatic mixed complexes. Mixed dimers are special class of clusters, where the geometries of the complexes are determined by the subtle balance between hydrogen bonding and dispersion interactions. As discussed earlier, there are extensive studies on aromatic clusters, which are stabilized by either

predominant electrostatic or dispersive interaction. Experimental studies of these mixed complexes in the literature is very scarce though there are few theoretical studies of these mixed complexes. The only mixed complex, which is studied experimentally is phenol dimer. It has been confirmed from various experimental as well as theoretical investigations that the geometry of the phenol dimer is stabilized by strong hydrogen bonding interaction as well as C-H…π, π-π, and dispersive interactions.[33-37] Thus, the aim of the present work is to investigate the intermolecular interactions in these systems experimentally as well as theoretically. It is also difficult to determine the structure of these complexes theoretically as conventional DFT functional does not include dispersion interaction and the MP2 calculations overestimate the dispersion interaction. Thus, it is challenging to study this special class of mixed complexes.

In this study we have investigated the structures of indole….furan dimer in a supersonic jet by using resonant two photon ionization (R2PI), Infrared-Ultraviolet (IR-UV) double resonance spectroscopic techniques and quantum chemistry calculations. There is no report of experimental as well as detailed theoretical studies of this complex in the literature.

Chapter 2

Methods

Laser based various experimental techniques as well as computational methods have been used to perform this work.

2.1. Experimental

2.1.1. Experimental set-up

The experiments have been performed in a home-built jet-cooled resonantly enhanced multiphoton ionization (REMPI) time of flight mass spectrometer (TOFMS) which is shown in Figure 1.

Figure1. Picture of home-built REMPI Time Of Flight Mass spectrometer

The setup consists of expansion and ionization chambers, where the operating pressures are 5 x 10^{-6} and 6 x 10^{-7} torr, respectively. The expansion chamber is pumped by a 10 in. diffstack diffusion pump (OD 250, Hind Hivac) and the ionization chamber is pumped by a 4.5 in. diffstack diffusion pump (OD 114, Hind Hivac). These two chambers are connected through a skimmer (Beam Dynamics Inc) of 2 mm diameter. The pulse valve of orifice diameter of 0.5

mm (General value, series 9, rep rate 10 Hz) is incorporated in the expansion chamber. 1m linear time of flight tube (Jordan TOF products) with a two-stage ion source of Wiley –Mclaren design is housed in the ionization chamber. It is pumped by a 4.5 in diffstack diffusion pump (OD 114, Hind Hivac). At the end of the time of flight tube a dual MCP (microchannel plate) detector, 18 mm in diameter is placed. This detector chamber is pumped by a 70 L/s turbo-molecular pump (Turbo-V81, Varian). The distance between nozzle to skimmer is fixed at 25 mm. The synthesis of mixed complexes of indole and furan as well as indole thiophene in supersonic jet has been discussed in the following.

A stainless steel sample holder is placed immediately behind the pulse valve. Indole (Sigma Aldrich) is taken in this holder and kept at temperature of 80^{o}C throughout the experiment. Furan is kept outside the vacuum chamber in a stainless steel sample holder. It has a high vapor pressure at room temperature. The temperature of furan is kept at -40^{o}C using $CaCl_2$ /dry ice cooling bath. Such a low temperature helps in maintaining desired flow of furan. Argon (Ar) at a pressure of 40 psig is used as a buffer gas. It is bubbled through furan and hence furan vapors seeded in Ar gas get mixed with indole and finally are expanded into vacuum through the pulsed nozzle.

The collimated molecular beam is ionized using one-color resonant two photon ionization (1C-R2PI) technique by frequency doubled output of a tunable dye laser (ND6000, Continuum) pumped by the second harmonic of a Nd:YAG laser (nanosecond, 10 Hz, Surelite II-10, Continuum). The resolution of the dye laser is about 0.08 cm^{-1}. Typical UV pulse energy used for ionization is about 0.4-0.5 mJ. The ions are mass analyzed in the time-of-flight mass spectrometer and detected by a 18 mm diameter dual MCP detector (Jordan TOF Products) placed at the end of the time-of-flight tube. The detector is housed in a small chamber. The ion signal from the detector is amplified using a preamplifier (SRS, Model SR445A) and sent to a digital oscilloscope (Tektronix, 350 MHz, DPO 4034) interfaced to a PC via an USB port. Both data acquisition and laser control are performed using home-built LabView (National Instruments, 8.6 Version) based programs. A schematic diagram of the experimental set-up has been shown in Figure 2.

IR spectrum of individual conformer of indole….pyridine heterodimer is measured using resonant ion dip infrared spectroscopy (RIDIRS). In this technique, two counter-propagating

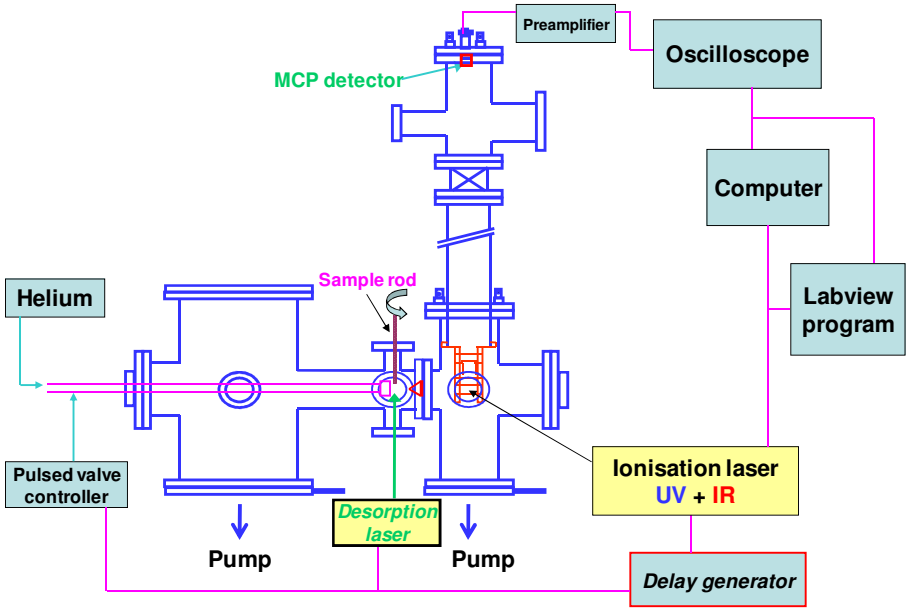

Figure 2. Schematic diagram of the experimental setup

IR and UV laser beams are spatially overlapped and intersected the molecular beam at right angle. Typical pulse energy of IR laser beam used is about 5-6 mJ and it is focused using a CaF_2 lens of focal length 185 cm, whereas the UV laser beam used is unfocused and the typical energy is about 0.4 mJ. IR laser, which is fired about 100 ns prior to the UV laser, is scanned through the vibrational transitions in the ground electronic state while the UV laser is fixed to a particular transition in the R2PI spectrum of the dimer. Thus IR spectra is obtained as depletion of the ion signal, whenever the IR laser frequency matches with any vibrational transition of the dimer in the ground electronic state. Further IR-UV hole-burning experiment is performed to discriminate the transitions in the R2PI spectrum, which belong to different conformers. This technique is just opposite to RIDIRS. Here the IR laser is kept fixed at a particular vibrational frequency of a conformer and the UV laser, which is fired after 50-100 ns from the IR laser, is scanned through the R2PI spectrum. As the IR laser would burn the population of a specific conformer through vibrational excitation, the UV excitation peaks of that conformer will show reduced intensity compared to those in the R2PI spectrum. On the other hand, the intensity of the UV excitation peaks of the other conformers in the R2PI spectrum will be unaltered even in

the presence of the IR beam. The tunable IR laser is a KTA based OPO (Laser Vision) pumped by an unseeded Nd:YAG laser (ns, 10Hz, Surelite II-10). Typical resolution of the IR laser used in the experiment is about 2-3 cm^{-1}.

2.1.2. Spectroscopic methods

Laser based various spectroscopic techniques, namely 1C-R2PI (one color resonant two photon ionization), RIDIRS (resonant ion dip infra-red spectroscopy), IR-UV hole-burning spectroscopic techniques have been used in the experiment. A schematic diagram of all these techniques has been shown in Figure 3.

a) Resonant 2 photon ionization (R2PI): In this technique, the molecules in rotationally and vibrationally cold supersonic molecular beam are excited from ground electronic state (S_0) to different vibrational levels of first excited electronic state (S_1) using a tunable ultraviolet (UV) laser and subsequently the second photon from the same laser beam ionizes the molecules. R2PI is coupled with time of flight mass analysis of the ions. Thus it provides mass selected electronic excitation spectra of different species (particularly clusters of different sizes) in the expansion while scanning the excitation wavelength.

b) RIDIRS: This technique is important to determine the structures of different conformations present in the R2PI spectrum by recording their infrared (IR) spectra without interference from others. Here the IR laser is fired 50-100 ns before the UV laser while the UV laser is fixed to a particular transition in the R2PI spectrum and the IR laser is scanned. There will be depletion of the ion signal whenever the IR laser frequency will be matching with any vibration of the molecule or the cluster.

c) IR-UV hole burning: This technique is just opposite to RIDIRS. Here the IR laser is kept fixed at a particular vibrational frequency of a conformer and the UV laser, which is fired after 50-100 ns from the IR laser, is scanned through the R2PI spectrum. As the IR laser will burn the population of a specific conformer through vibrational excitation, the UV excitation peaks of that conformer will show reduced intensity compared to those in the R2PI spectrum while the intensity of the UV excitation peaks of the other conformers will be unaltered.

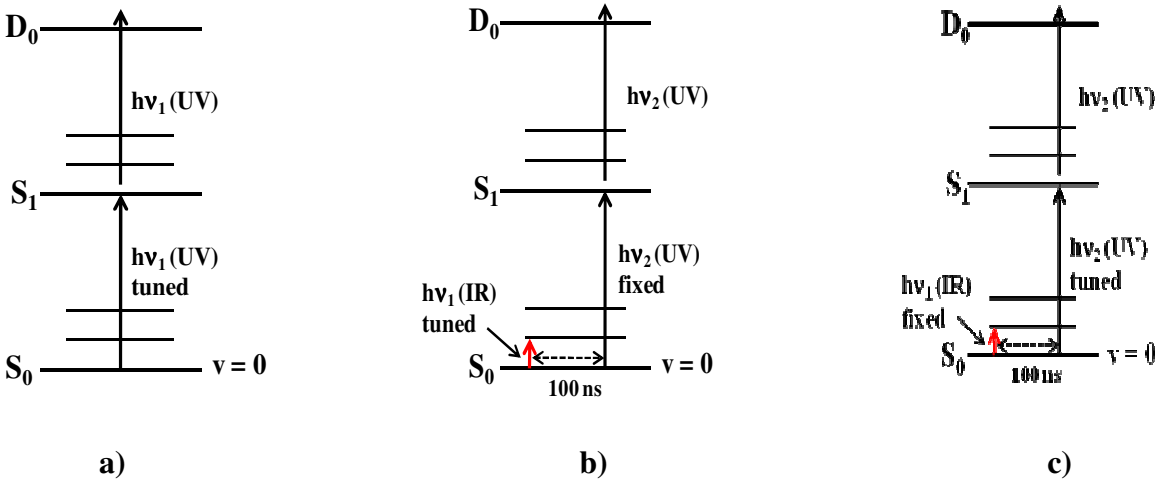

Figure 3. The schematic diagram for the principle of R2PI, RIDIRS and IR-UV hole spectroscopy.

2.1.3. Principle of cooling

Supersonic expansion of molecules help to attain a suitable environment for carrying out experiments using an inert monoatomic gas (carrier gas). The first step is the expansion of the carrier gas which results in lowering of the translational temperature to a value as low as 0.03K. When polyatomic molecules are seeded into this carrier gas, the interaction causes the translational and rotational degree of freedom to cool to few kelvin. The carrier gas acts as cooling bath where the interaction happens via two body collisions. In this process, three-body collisions are minimized to such an extent that condensation does not take place. Vibrational cooling is also extensive but lesser compared to translational and rotational cooling. Generally translational cooling is around 0.1-10K and vibrational cooling ranges from 20-150K. A supersonic jet results in cold, isolated gas phase molecules. Principle of expansion is show in Figure 4.

High pressure gas is expanded from a reservoir into vacuum through a small orifice. As shown in the figure the motion is random before the orifice. After the orifice the mass flow becomes directional. High resolution spectroscopy makes use of supersonic jets as the molecules are cold, isolated and their density is high and the disadvantage of intermolecular perturbation is

not there. Thus, study of molecules in supersonic jet provides highly resolved electronic spectra as well as opportunities to investigate the structures of weakly bound clusters of specific sizes.

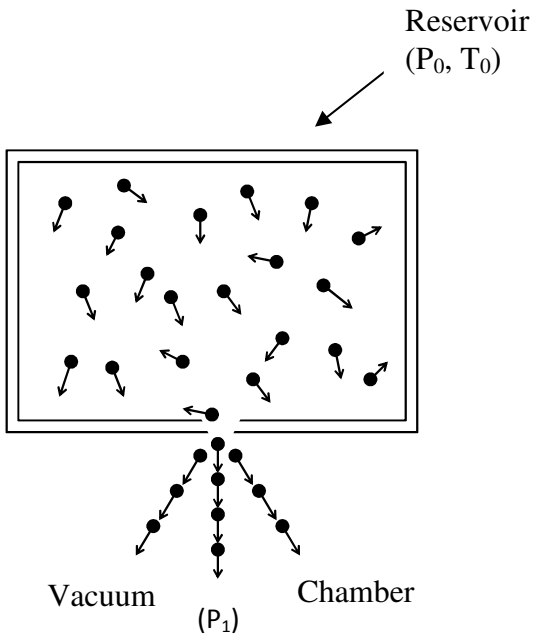

Figure 4. Conversion of random motion into a direct mass flow. P_0 is the reservoir pressure and P_1 is the background pressure of the vacuum chamber. Mean-Free path between collisions is less than the orifice diameter.

2.2. Computational

Starting geometries of all possible conformers of indole...furan dimer is optimized initially using M05-2X/6-31+G* level of theory. The output of this basis set is further optimized at DFT/M05-2X, DFT/M06-2X using cc-pVDZ and aug-cc-pVDZ basis sets and MP2 levels using cc-pVDZ basis set for both the dimers. In optimization of the conformers "ultrafine" numerical integration grid is used to obtain reliable results. The calculation of harmonic vibrational frequency for all the conformers is done at DFT/M05-2X using aug-cc-pVDZ basis set, at DFT/M06-2X and MP2 levels using cc-pVDZ basis set. The binding energies for all the conformers are corrected for basis set superposition error (BSSE) and zero point vibrational energy. BSSE correction is done using the counterpoise method given by Boys and Bernadi.[38] MP2 and DFT/M05-2X calculations are performed using Gaussian 03 program package[39] and NWChem software[40] are used for DFT/M06-2X calculations.

Chapter 3

Results and discussion

3.1. Time of flight (TOF) mass spectrum

Figure 5 shows TOF mass spectrum of complexes of indole and furan recorded at 35196 cm^{-1}, which is the origin band position of indole…furan dimer. The mass peak observed at 185 amu is due to indole…furan dimer. Other higher clusters of indole such as $(indole)_2$, $(indole)_3$, indole…$(furan)_2$ and indole…$(furan)_3$ are also observed in the mass spectrum. Water is present as an impurity in the sample leading to the formation of cluster of indole and water. Ar at 40 psig is used as a buffer gas.

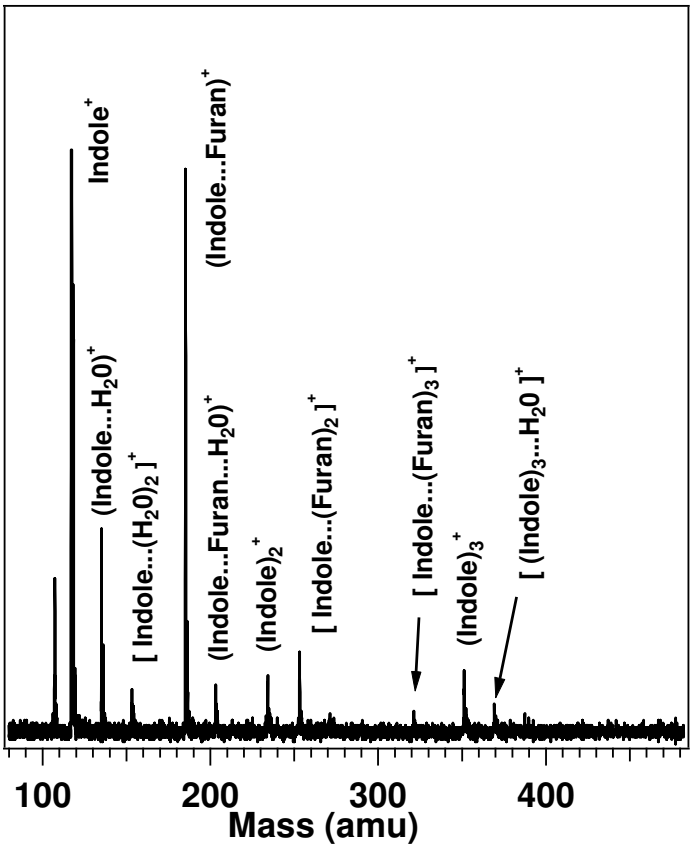

Figure 5. TOF mass spectrum of indole in presence of furan.

3.2. Resonant 2-photon ionization (R2PI) spectra

One-color R2PI spectrum of indole in absence of furan is shown in Figure 6(a). The origin band (0_0^0) for the $S_1 \leftarrow S_0$ electronic transition appears at 35240 cm^{-1}, which is reported previously.[41] Figure 6(b) shows one-color R2PI spectrum recorded in indole…furan dimer mass channel. The band at 35196 cm^{-1} has been assigned as the origin band of indole…furan dimer. The R2PI spectrum in Figure 6(b) shows a prominent band at 32 cm^{-1} which is assigned as low frequency intermolecular vibration of the dimer. The origin bands of both monomer and dimer are set to zero of the frequency scale to compare the intramolecular vibrational frequencies of the monomer and the dimer. The origin band of the dimer is red-shifted by about 44 cm^{-1} from that of the indole monomer. The high frequency vibrations observed at the blue side of 0_0^0 band of the dimer are compared with the monomer R2PI spectrum. The comparison shows that all the peaks except the 32 cm^{-1} one observed in the blue side of the origin band of the dimer are due to intramolecular vibrations of the monomer unit. There is little change in the frequencies of the intramolecular vibrations of indole in the complex compared to that in the monomer due to complex formation of indole with furan.

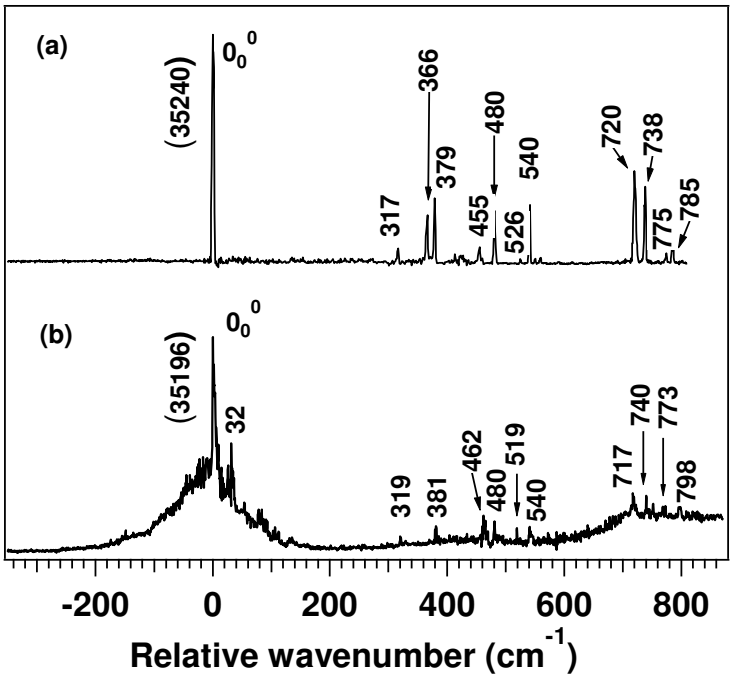

Figure 6. One-color R2PI spectra recorded in a) indole monomer, b) indole…furan dimer mass channels. The respective electronic origins have been considered as zero of the frequency scale.

Generally, the amount of red-shift in the band origin of the complex with respect to that of the monomer indicates the extent of stability of the complex in the excited electronic state. It is interesting to compare the stability of indole…furan dimer with the hydrogen bonded indole...water complex. The red shift in the bond origin of indole…water complex is 132 cm^{-1}, which indicates that indole…water dimer is much stronger than indole…furan complex.[42] Smaller red-shift in the band origin of indole…furan complex compared to indole…water could be due to participation of lone pair electron of the oxygen atom in the aromaticity of the furan ring. Although it should be noted that the lone pair electron of oxygen atom of furan is partially mixed with the π-orbital of the ring as the atomic orbital of the oxygen atom is an sp^3 type.

A broad background underneath the origin band of indole…furan dimer is observed in the R2PI spectrum recorded in the indole…furan dimer mass channel. Similar but relatively weak background is observed near the 717 cm^{-1} vibronic band of the dimer. The origin of the background can be due to an isomer complex of the dimer or due to a higher cluster which is fragmenting into the dimer mass channel. R2PI spectrum has been recorded in the indole…$(furan)_2$ trimer mass channel and the spectrum nicely reproduces the background observed in the dimer mass channel. Thus, the background obtained in the R2PI spectrum recorded in the dimer mass channel is due to electronic excitation of indole…$(furan)_2$ trimer which is fragmenting into the dimer mass channel.

3.3. RIDIR spectra

The determination of the structure of the indole…furan dimer is done through IR-UV double-resonance technique by probing the electronic transitions observed in the R2PI spectrum. Figure 7(a) shows the RIDIR spectrum of indole monomer, where the NH stretch fundamental of indole monomer appears at 3526 cm^{-1}, which agrees very well with the previous report.[43] Figure 7(b) shows the RIDIR spectrum in the N-H stretch region by probing origin band of indole…furan dimer.

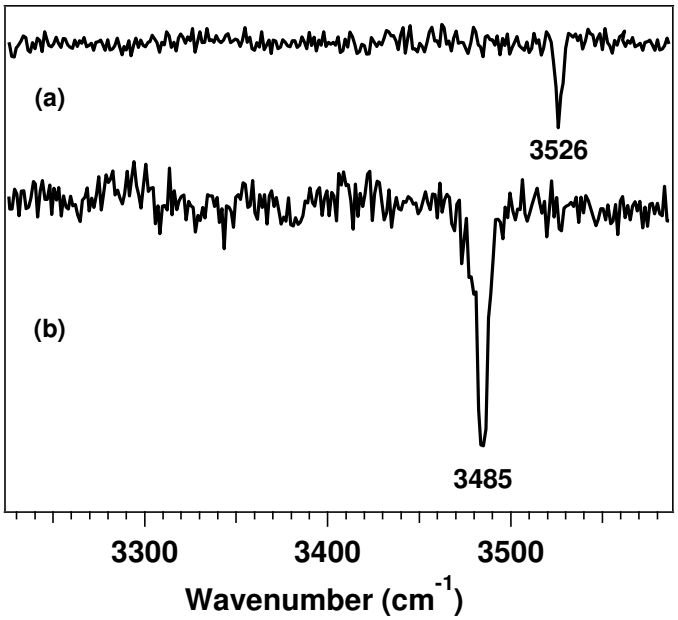

Figure 7. RIDIR spectra by probing (a) 0_0^0 band of indole , (b) 0_0^0 band of indole furan dimer. We observe only a single conformer in our system.

A single band is observed at 3485 cm^{-1}, is assigned as the N-H stretching vibration of the dimer. The N-H stretching vibration of indole…furan dimer is red-shifted by 41 cm^{-1} compared to that of indole monomer. In case of indole…water complex, the red-shift in the N-H stretching vibration compared to that of indole monomer is 89 cm^{-1}. Thus, the RIDIRS data show the similar trend like the R2PI data that hydrogen bond in the indole…furan complex is weaker than that in indole…water complex.

To confirm the presence of only one conformer of the dimer, in the experiment, IR spectra by probing most of the electronic transitions in the R2PI spectrum have been recorded. RIDIR spectra by probing 0_0^0+32 cm^{-1}, 0_0^0+480 cm^{-1}, and 0_0^0+740 cm^{-1} electronic bands of the dimer have been shown in Figure 8(b)-(d).

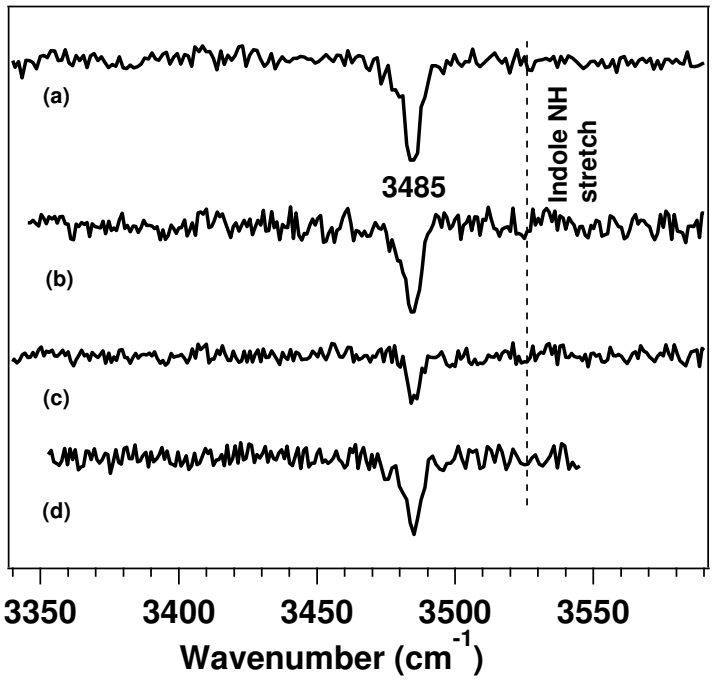

Figure 8. RIDIR spectra by excitation at (a) 0_0^0, (b) 0_0^0 + 32 cm^{-1}, (c) 0_0^0 + 480 cm^{-1}, and (d) 0_0^0 + 740 cm^{-1} bands of indole…furan dimer.

The IR spectrum by exciting origin band of the dimer is shown in Figure 8(a) for comparison with the spectra provided in Figure 8(b)-(d). Identical IR spectra in all the cases confirm the presence of only one conformer of the dimer in the experiment.

3.4. IR-UV hole-burning spectra

IR-UV hole-burning spectrum by probing the vibrational band of the dimer at 3485 cm^{-1} observed in the RIDIR spectra is shown in Figure 9(a). Figure 9(b) shows the R2PI spectrum of the cluster of indole and furan recorded in the dimer mass channel, which is already presented in Figure 6(b).

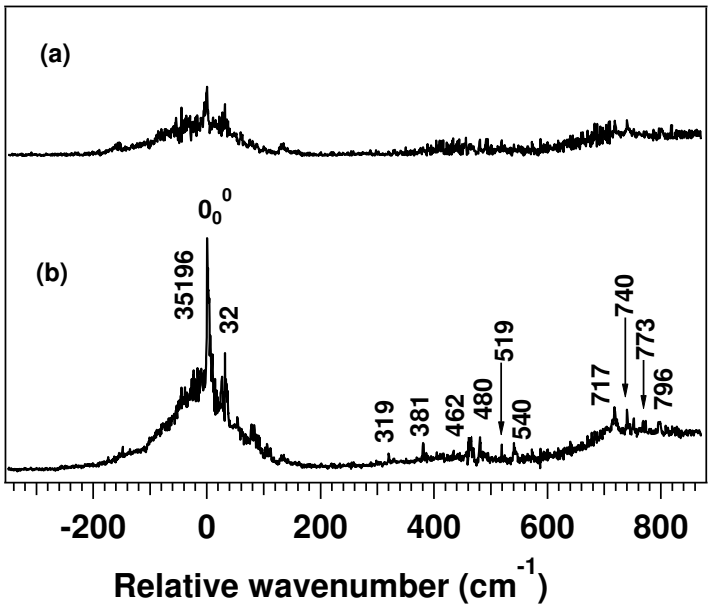

Figure 9. (a) IR-UV hole-burning spectrum recorded in the indole…furan dimer mass channel by pumping the vibrational band at 3485 cm^{-1}, (b) R2PI spectrum in the indole…furan dimer mass channel. The respective electronic origins have been considered as zero of the frequency scale.

IR-UV hole-burning spectrum shows the dip in ion signals for all the electronic bands in the R2PI spectrum shown in Figure 9(b) except the broad background observed near the origin band as well as 717 cm^{-1} vibronic band of the dimer. Thus it is confirmed that only one conformer of the dimer is present in the experiment and the broad background observed in the R2PI spectrum of the dimer is due to electronic transition of different species. It has been already confirmed in the section 3.1.3. that the broad background observed in the R2PI spectrum recorded in the dimer mass channel is due to electronic transition of trimer only.

3.5. Theoretical Results

The possible structures of indole…furan dimer with different orientations of the monomer units are shown in Figure 10. These structures have been used as initial geometries for optimization at different levels using various basis sets.

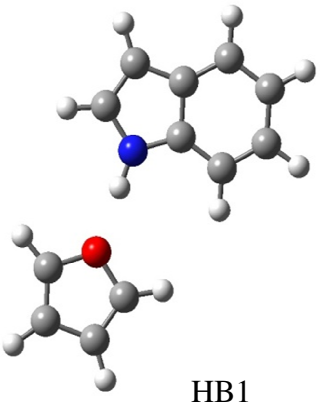

HB1

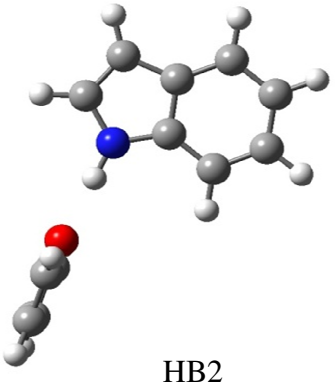

HB2

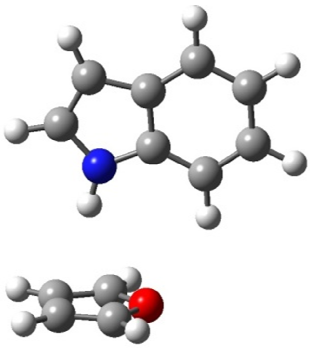

NH…π

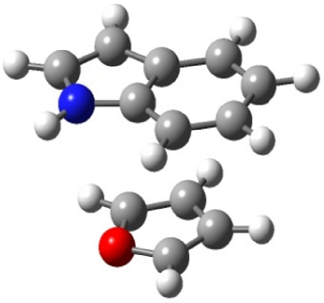

Syn-PD

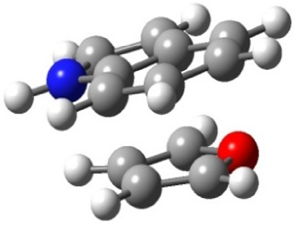

Anti-PD

Figure 10. Structures of possible conformers for indole…furan dimer. These structures are used as initial geometries for optimization.

As shown in Figure 10, we have considered five possible geometrical isomers of three different categories namely hydrogen bonded (HB1 and HB2), N-H…π and parallel displaced π-stacked (syn and anti). In both HB1 and HB2 structures, there is a σ-type hydrogen bond between NH group of indole and oxygen atom of furan. But in case of HB2, indole and furan are oriented in perpendicular fashion to each other through N-H…O hydrogen bond, whereas in HB1 indole and furan are in the same plane. The third geometric conformer named N-H…π shows the interaction between NH group of indole and the π-cloud of the furan ring. Anti-PD and Syn-PD are parallel displaced π-stacked conformers. In case of Anti-PD, indole NH group and oxygen atom of furan are oriented in the opposite side. But indole NH group and oxygen atom of furan are facing same side in case of Syn-PD conformer.

As most of the structures of the dimer shown in Figure 10 are stabilized by electrostatic as well as dispersion interactions, optimization is mostly done using density functional theory (DFT) with M05-2X and M06-2X functional. Recently Zhao and Truhlar have developed these meta-density functional which prove significantly improved results for non-covalently bonded complexes having dispersion interactions.[44] Various structures of the dimer have been optimized at the MP2 level as well although MP2 theory overestimates the dispesion interaction. All the five possible geometries of the dimer have been optimized initially at M05-2X/6-31G level of theory. The optimization of both HB1 and HB2 led to a stable V-shaped hydrogen bonded geometry shown in Figure 11(b). It has been found that neither HB1 nor HB2 structures are stable. The planar HB1 structure is unstable due to steric repulsion of adjacent hydrogen atoms of indole and furan rings. HB2 structure with pure electrostatic (N-H…O hydrogen bonding) interaction is also not stable because there is possibility of having simultaneous dispersion interaction in addition to hydrogen bonding interaction.

Figure 11(a) shows atom-numbering scheme used in geometry optimization of indole…furan dimer and this numbering scheme is used to compare important calculated geometric parameters of various conformers of the dimer. The structures of four conformers of the dimer optimized at M05-2X/aug-cc-pVDZ level have been shown in Figure 11(b).

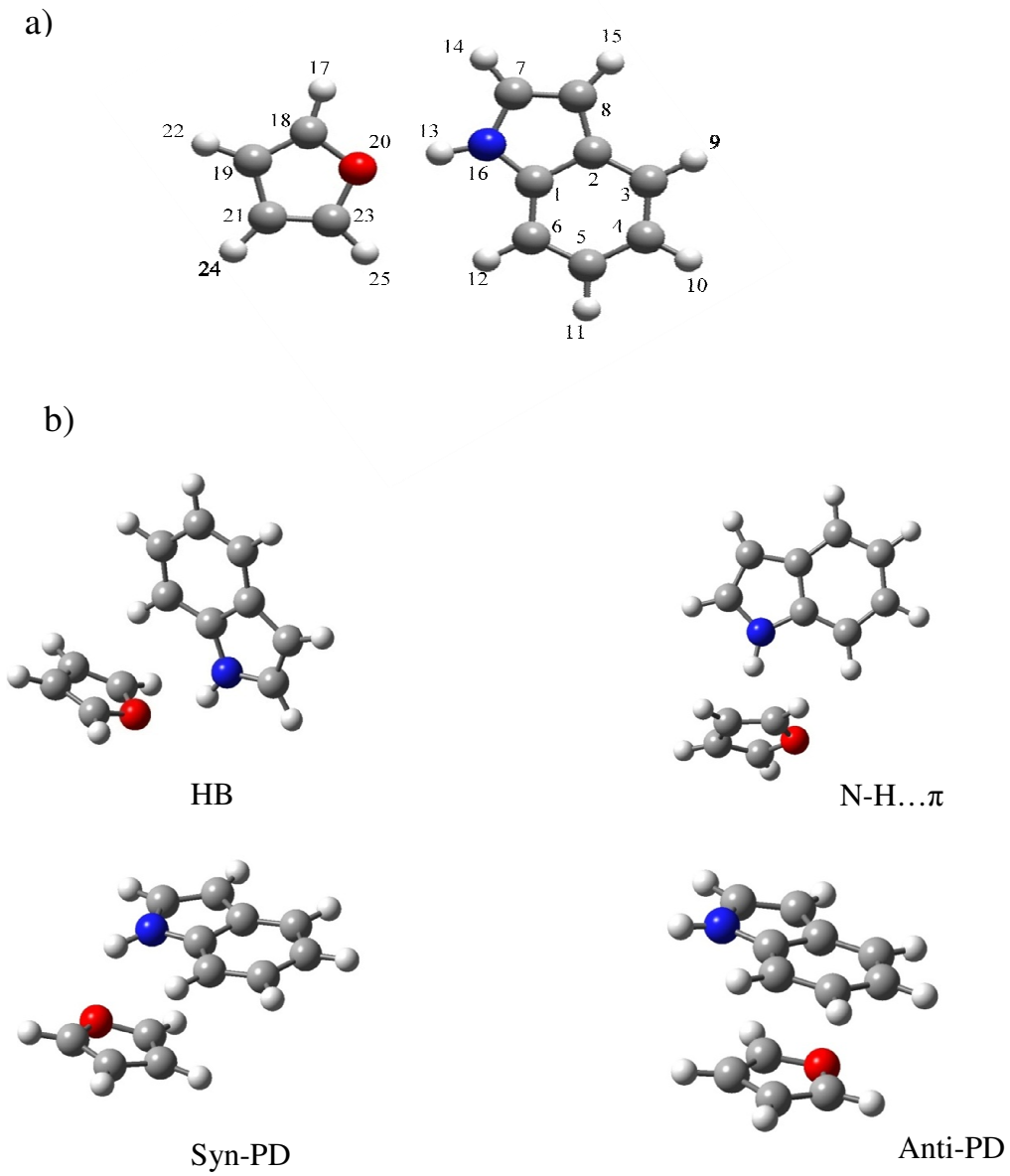

Figure 11. (a) Atom-numbering scheme in iodole…furan dimer and (b) M052X/aug-cc-pVDZ optimized structures of four conformers. The geometrical parameters of these optimized structures are shown in Table 2.

Table 1 shows few selected geometric parameters of the four conformers of the dimer calculated at M05-2X/aug-cc-pVDZ level of theory. The V-shaped HB conformer possesses a N-H…O hydrogen bond with H…O distance ($d_{N\text{-}H\ldots O}$) of 2.18 Å, N…O distance ($d_{N\ldots O}$) of 3.08 Å, and <N-H-O of 148^0. Very small increase in the N-H bond length ($\Delta r_{N\text{-}H}$ = 0.0013 Å) of

indole upon formation of dimer with furan indicates formation of very weak hydrogen bond in the V-shaped HB conformer. Although the geometry of this conformer is characterized mostly by N-H…O hydrogen bonding interaction, the geometry is stabilized by additional weak C-H…O ($d_{C\text{-}H\ldots O}$ = 2.78 Å) electrostatic interaction as well as dispersive interaction through C-H…π ($d_{C\text{-}H\ldots\pi}$ = 2.62 Å) hydrogen bonding and weak parallel-displaced π-π interaction. Due to the presence of additional electrostatic and dispersive interactions in the HB conformer, the geometry is not perfectly perpendicular to each other through N-H…O hydrogen bond but the two monomer units are bent to each other forming a unique V-shape structure. The wagging angle (<$C_6C_1N_{16}H_{13}$) between the two rings is -58.5^0. Similar kind of V-shaped geometry has been reported for phenol dimer[36] as well as indole…pyridine dimer.[45]

Table 1. Few selected geometrical parameters of all the optimized geometries of the four conformers at M052X/aug-cc-pVDZ level of theory.

	HB (V-shaped)	N-H...π	Syn-PD	Anti-PD
$d_{N\text{-}H\ldots O}$ (Å)	2.182	2.646	2.84	--
$d_{N\ldots O}$ (Å)	3.08	3.44	3.225	--
$\Delta r_{N\text{-}H}$ (Å)	0.0013	0.0024	0.0015	0.0008
<N-H…O	147.7^0	136.32^0	103.05^0	--
[a]<$C_6C_1N_{16}H_{13}$	- 0.726^0	3.22^0	-11.15^0	-1.11^0
Interplanar distance (Å)	--	--	3.2	3.52
[a]<$C_1N_{16}O_{20}C_{18}$	58.5^0	-152.21^0	86.74^0	154.29^0
$d_{C\text{-}H\ldots O}$ (Å)	2.78	2.654	--	--
<C-H…O	126.48^0	135.65^0	84.23^0	--
$d_{C\text{-}H\ldots\pi}$ (Å)	2.62	--	--	--
$d_{N\text{-}H\ldots\pi}$ (Å)	--	2.38	2.69	--

[a]For atom numbering of the dimer, see figure 7(a).

Two types of parallel-displaced (PD) π-stacked structures of the dimer, syn-PD and anti-PD, have been obtained after geometry optimization. There is a striking difference in the

geometry of these two parallel-displaced structures. The monomer units in the anti-PD structure is perfectly parallel with an interplanar distance of 3.52 Å. In case of anti-PD structure, indole N-H group and oxygen atom of furan are oriented opposite to each other without having any possibility of hydrogen bonding interaction. On the other hand, both indole N-H group and oxygen atom of furan are in the same side forming weak N-H…O hydrogen bond with N-H…O distance of 2.84 Å for syn-PD. Due to this hydrogen bonding interaction, hydrogen atom of NH group of indole moves out of plane to significant extent. The two monomer units are also no more parallel to each other, rather the pyrrole group of indole and furan are inclined to each other providing an interplanar distance of 3.2 Å. The out of plane angles of N-H group ($<C_6C_1N_{16}H_{13}$) of inole moiety for bare indole, syn-PD, and anti-PD are 0^0, -11.2^0, and -1.1^0 respectively. Significant extent of non-planarity of the indole N-H group in the syn-PD dimer favors for reasonable hydrogen bonding interaction in the π-stacked dimer. N-H…π distance of 2.69 Å is also present in syn-PD structure. Thus, syn-PD dimer has a unique stacked structure which is stabilized by π-stacking and N-H…π dispersion interactions as well as weak electrostatic interaction. The T-shaped N-H…π bound dimer is also stabilized by dispersion interaction (N-H…π) as well as electrostatic interactions through N-H…O and C-H…O hydrogen bonding. The N-H…π, N-H…O, and C-H…O distances in the N-H…π conformer are 2.38 Å, 2.64 Å, and 2.65 Å, respectively.

The zero point energy (ZPE) corrected relative energies as well as BSSE and ZPE corrected binding energies for all the four conformers of the dimer calculated at various levels of theory using different basis sets are presented in Table 2. At M06-2X/aug-cc-pVDZ level of theory, binding energy of the dimer is corrected only for BSSE and relative energy of the dimer is also not corrected for ZPE. Comparison of ZPE corrected relative energies of various conformers of the dimer shows that syn-PD conformer is the global minimum at most of the levels of the theory. But it is true that the differences in relative energies among syn-PD, NH…π, and HB conformers are very small. Binding energies of these three conformers calculated at M05-2X/aug-cc-pVDZ and MP2/cc-pVDZ levls are also very close to each other. But calculations at M06-2X/cc-pVDZ level show that binding energy of syn-PD conformer is about 1 kcal/mol higher than that of both NH… π and HB conformers of the dimer. The relative energies (ZPE corrected) of the NH… π and HB conformers are also about 1 kcal/mol and 0.4 kcal/mol, respectively higher than that of syn-PD conformer.

Table 2. BSSE and ZPE corrected binding energies (kcal/mol) of four conformers of indole…furan dimer at various level of theory.

	M05-2X/ aVDZ			M06-2X/ cc-pVDZ			M06-2X/ aVDZ		MP2/ cc-pVDZ		
	ΔE_e	ΔE_0	E_{rel}	ΔE_e	ΔE_0	E_{rel}	ΔE_e	E_{rel}*	ΔE_e	ΔE_0	E_{rel}
HB (V-shaped)	- 4.10	-3.39	0.32	- 6.50	-4.75	0.42	-4.86	0.00	-3.57	-2.92	0.040
NH…π	- 3.99	-3.51	0.15	- 6.33	- 4.12	0.98	-4.10	0.71	-3.75	-3.29	0.003
Syn-PD	- 3.82	-3.52	0.00	- 6.88	- 5.69	0.00	-4.17	0.44	-3.13	-2.70	0.000
Anti-PD	-2.10	-1.95	1.44	-5.62	-3.88	1.44	-3.96	0.73	-1.62	-1.41	0.747

ΔE_e: BSSE corrected binding energy, ΔE_0: BSSE + ZPE corrected binding energy, E_{rel}: ZPE corrected relative energy, E_{rel}*: ZPE uncorrected relative energy.

It is already indicated in the discussion of the geometrical parameters of the various conformers of indole…furan dimer that conventional hydrogen bonding interaction (N-H…O) in the HB conformer is quite weak. Thus it is quite challenging to determine the most stable conformer among HB, NH… π, and syn-PD when all of the three structures are stabilized by electrostatic and dispersion interactions. It is confirmed from the experiment that only one conformer of the dimer is observed in the gas phase. On the basis of M06-2X/cc-pVDZ calculations, the observed dimer in the experiment can be assigned as syn-PD. Further proof of this assignment has been provided in the following sections.

The strength of the hydrogen bond interaction in a complex can be explained theoretically on the basis of natural bond orbital (NBO) analysis. In this analysis, hydrogen bonding interaction in X-H…A system is described by charge transfer delocalization between the lone pair of the hydrogen bond acceptor A and the antibonding σ*(X-H) orbital of the donor. $E^{(2)}_{i\rightarrow j^*}$ is the second-order perturbative energy, which is used to estimate the energy decrease caused by the electron delocalization in hydrogen bonding interaction, where i and j^* indicates a lone pair orbital and an antibonding σ* orbital, respectively. This energy is approximately proportional to the overlap integral between the lone pair orbital of A and the antibonding σ*(X-H) orbital. In case of hydrogen bonding interaction with oxygen atom as hydrogen bond acceptor, there are possibilities of two types of delocalization interactions between n_σ (σ type) and n_p (p type) lone pair orbitals of oxygen and the antibonding σ*(X-H) orbital. Recently dual hydrogen bonding interaction in 1:1 complex of indole and N-methylacetamide has been

reported by Sakota et al.[46] It will be interesting to determine the hydrogen bonding interaction in indole…furan dimer using NBO analysis.

Table 3. Natural bond orbital analysis of hydrogen-bonded conformer of indole…furan dimer and comparison with other complexes. The calculation is done at M05-2X/aug-cc-pVDZ level of theory.

	Indole…furan HB (V-shaped)	Indole…water[a] HB	Indole… (N-methylacetamide)[b] HB
$\Delta q(H)$	0.0198	0.0329	
$\Delta q(O)$	-0.0235	-0.0149	
$\delta(n_O)$	1.969	1.994	
$\delta(\sigma^*_{N-H})$	0.0239	0.0291	
$E_{i\rightarrow j^*}^{(2)}$ (kcal/mol) $(n_\sigma \rightarrow \sigma^*_{NH})$	1	10.4	8.29
$E_{i\rightarrow j^*}^{(2)}$ (kcal/mol) $(n_p \rightarrow \sigma^*_{NH})$	3.2	0.15	7.17
$\Delta\nu_{NH}\,(cm^{-1})$ (experimental)	-41	-89	-218

[a]Reference 42. [b]Reference 46. The value calculated for indole…furan dimer and indole…water dimer is at MO5-2X/aug-cc-pVDZ level of theory. The values for indole…(N-methylacetamide) dimer is from B3LYP/6-311++G** level of theory. In this case $\Delta q(H)$, $\Delta q(O)$, $\delta(n_O)$ and $\delta(\sigma^*_{N-H})$ values are not available.

The results of NBO calculations for indole…furan dimer performed at M05-2X/aug-cc-pVDZ level of theory have been presented in Table 3 and the data have been compared with indole…H_2O and indole…N-methylacetamide, where similar N-H…O interaction is present. The experimental red shift in the N-H stretching frequency of each of the three indole complexes is also provided in Table 3 to compare with the magnitude of $E^{(2)}_{i\rightarrow j^*}$. The changes in the atomic charges on H atom of hydrogen bond donor group i.e. N-H group of indole and oxygen atom (hydrogen bond acceptor) are denoted by $\Delta q(H)$ and $\Delta q(O)$, respectively. The occupancy in the

lone pair orbital of oxygen atom is denoted by $\delta(n_O)$ and that for antibonding orbital is denoted by $\delta(\sigma^*_{N-H})$. In case of indole…N-methylacetamide complex, $E^{(2)}_{i\rightarrow j^*}$ energies for both $n_\sigma \rightarrow \sigma^*_{N-H}$ and $n_p \rightarrow \sigma^*_{N-H}$ are quite large leading to strong dual hydrogen bonding interactions. On the other hand, indole…H_2O cluster shows a large $E^{(2)}_{i\rightarrow j^*}$ energy for $n_\sigma \rightarrow \sigma^*_{N-H}$ interaction but $E^{(2)}_{i\rightarrow j^*}$ value for $n_p \rightarrow \sigma^*_{N-H}$ is very small (0.2 kcal/mol). The red shifts in the N-H stretching frequency of indole…H_2O and indole…N-methylacetamide complexes are 89 and 218 cm^{-1} respectively. Very large amount of red shift in the N-H stretching frequency of indole…N-methylacetamide complex compared to that of indole…H_2O complex has been explained in terms of strong dual hydrogen bonding interaction in the former case. For the hydrogen bonded (HB) conformer of indole…furan dimer, $E^{(2)}_{i\rightarrow j^*}$ energy for $n_\sigma \rightarrow \sigma^*_{N-H}$ interaction is very small (1 kcal/mol) compared to that for indole…H_2O complex (10.4 kcal/mol). $E^{(2)}_{i\rightarrow j^*}$ value for $n_p \rightarrow \sigma^*_{N-H}$ interaction in indole…furan hydrogen bonded dimer is 3.2 kcal/mol. Overall second order perturbative energy for indole…furan HB dimer indicates the presence of very weak hydrogen bond. Small red shift (41 cm^{-1}) observed in the N-H stretching frequency of indole…furan complex is thus nicely explained in terms of NBO analysis.

To determine the structure of the conformer of indole…furan dimer observed in the experiment, N-H stretching frequency (ν_{N-H}) of the four possible conformers has been calculated at different levels of theory and listed in Table 4.

Table 4. The scaled NH stretching vibrational frequencies for all the four possible conformers at different levels of theory.

	M05-2X/aVDZ	M06-2X/cc-pVDZ	MP2/cc-pVDZ
	ν_{N-H} (Int)	ν_{N-H} (Int)	ν_{N-H} (Int)
HB (V-shaped)	3493(252)	3510(245)	3495(250)
NH…π	3476(316)	3487(227)	3479(353)
Syn-PD	3489(104)	3478(117)	3479(124)
Anti-PD	3531(85)	3529(167)	3526 (81)

Intensity in km/mol is given in bracket. Frequencies have been scaled by a factor of 0.94, 0.95 and 0.96 for M05-2X/aVDZ, M06-2X/cc-pVDZ and MP2/cc-pVDZ basis sets respectively.

Theoretical N-H stretching frequency values obtained at every level of theory and basis set are scaled using a scaling factor obtained from the ratio of theoretical and experimental N-H stretching frequencies of indole monomer. Experimental N-H stretching frequencies of indole monomer and indole…furan dimer are 3526 and 3485 cm^{-1}, respectively. Comparison of theoretical N-H stretching frequencies of all the four conformers of the dimer obtained at different levels of theory with the experimental N-H stretching frequency of the dimer reveals that N-H stretch frequencies of both syn-PD and N-H…π conformers are very close to the observed frequency of the dimer. Figure 12 shows experimental IR spectrum of indole…furan dimer and theoretical IR spectra of the four conformers of the dimer calculated at M06-2X/cc-pVDZ level of theory.

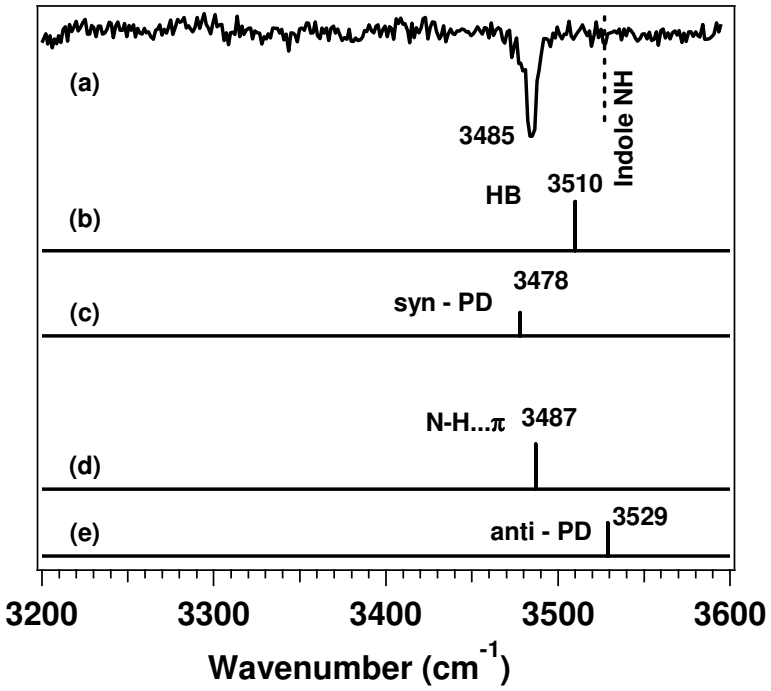

Figure 12. RIDIR spectra by probing (a) 0_0^0 band of indole…furan dimer. Theoretical IR spectra for all the four conformers calculated at M06-2X/cc-pVDZ level of theory are provided in figure 10(b-e).

Similar N-H stretching frequencies of syn-PD, N-H…π, and even HB conformers can be due to presence of multiple similar interactions (electrostatic as well as dispersion) in all the three conformers. As for example, apart from N-H…π interaction, N-H…π conformer is

stabilized due to N-H…O and C-H…O interactions. Similarly, Syn-PD conformer is stabilized by N-H…O, and N-H…π interactions in addition to π-stacking interactions. As syn-PD conformer has highest binding energy, the structure of the observed dimer is assigned as syn-PD. It is interesting to note that the parallel displaced stacked dimer becomes the most stable conformer due to collective interactions of stacking, N-H…π, and N-H…O. This is quite reasonable when the N-H…O interaction is very weak in the conventional hydrogen bonded conformer. The stability due to these kinds of multiple interactions is very often found in the biological systems.

3.6. Conclusions

Intermolecular interactions in indole…furan dimer have been investigated in a supersonic jet using one-color R2PI, IR-UV double resonance spectroscopic techniques combined with DFT and ab initio calculations. R2PI spectrum of the dimer has been measured by electronic excitation of the indole moiety. The electronic origin band of the dimer is red sifted from the 0_0^0 band for the $S_0 \rightarrow S_1$ transition of the indole monomer by 44 cm^{-1}. A broad background underneath the origin transition of the dimer has been assigned as the electronic transition band of the trimer by recording R2PI spectrum in indole…$(furan)_2$ trimer mass channel. RIDIR spectrum of the dimer shows red shift in the N-H stretching frequency of the dimer by 41 cm^{-1}. The presence of only one conformer of the dimer has been confirmed from IR-UV hole-burning spectroscopy. DFT/M05-2X, DFT/M06-2X as well as MP2 level calculations predict four low energy conformers of the dimer. It has been found that three conformers of the dimer (hydrogen bonded, syn-PD and N-H…π) are stabilized by similar kinds of multiple electrostatic and dispersion intermolecular interactions. Comparison of theoretical IR spectra of the four conformers of the dimer with experimental IR spectra shows that N-H stretching frequencies of both syn-PD and N-H…π conformers are very close to that of the observed dimer. NBO calculation shows that hydrogen bonding interaction in the HB conformer is very weak. Binding energy calculations of the dimer at DFT/M06-2X level show that syn-PD conformer is the global minimum. Thus the structure of the experimentally observed dimer has been assigned as syn-PD, where the geometry is stabilized by N-H…O, N-H…π, and π-stacking interactions. Present study on indole…furan system nicely demonstrates the competition among multiple intermolecular interactions present in a conformer, which stabilize the geometry of the dimer.

References

(1) Saenger, W. *Principles of Nucleic Acid Structure*; Springer-Verlag: New York, 1984.

(2) Meyer, E. A.; Castellano, R. K.; Diederich, F. *Angew. Chem., Int. Ed.* **2003**, *42*, 1210.

(3) Desiraju, G. R. *Angew. Chem., Int. Ed.* **1995**, *34*, 2311.

(4) Lehn, J.-M. *Supramolecular Chemistry: Concepts and Perspectives*; VCH: New York, 1995.

(5) Hoeben, F. J. M.; Jonkheijm, P.; Meijer, E. W.; Schenning, A. P. H. *Chem. Rev.* **2005**, *105*, 1491.

(6) Sygula, A.; Fronczek, F. R.; Sygula R.; Rabideau, P. W.; Olmstead M. M. *J. Am. Chem. Soc.* **2007**, *129*, 3842.

(7) Pauling, L. *The nature of chemical bond*; Cornell University Press, Ithaca, New York, 1939.

(8) Pimental, G.C. and McClellan, A.L. *The hydrogen Bond*. W.H. Freeman, San Francisco, 1960.

(9) Steiner, T.; Saenger, W. *Journal of the American Chemical Society* **1993**, *115*, 4540.

(10) Fraser, G. T.; Lovas, F. J.; Suenram, R. D.; Gillies, J. Z.; Gillies, C. W. *Chemical Physics* **1992**, *163*, 91.

(11) Keegstra, E. M. D.; Spek, A. L.; Zwikker, J. W.; Jenneskens, L. W. *Journal of the Chemical Society, Chemical Communications* **1994**, 1633.

(12) Lewis, F. D.; Yang, J.-S.; Stern, C. L. *Journal of the American Chemical Society* **1996**, *118*, 12029.

(13) Wulf, O. R.; Liddel, U.; Hendricks, S. B. *Journal of the American Chemical Society* **1936**, *58*, 2287.

(14) Elsaesser, T. *Accounts of Chemical Research* **2009**, *42*, 1220.

(15) Marczak, W.; Kielek, K.; Czech, B.; Flakus, H.; Rogalski, M. *Physical Chemistry Chemical Physics* **2009**, *11*, 2668.

(16) Zwier, T. S. *Annual Review of Physical Chemistry* **1996**, *47*, 205.

(17) Oikawa, A.; Abe, H.; Mikami, N.; Ito, M., *The Journal of Physical Chemistry*, **1983**,

87, 5083

(18) Schiefke, A.; Deusen, C.; Jacoby, C.; Gerhards, M.; Schmitt, M.; Kleinermanns, K.; Hering, P. *Journal of Chemical Physics* **1995**, *102*, 9197.

(19) Nakanaga, T.; Kawamata, K.; Ito, F. *Chemical Physics Letters* **1997**, *279*, 309.

(20) Nakanaga, T.; Sugawara, K.; Kawamata, K.; Ito, F. *Chemical Physics Letters* **1997**, *267*, 491.

(21) Nakanaga, T.; Ito, F. *Journal of Physical Chemistry A* **1999**, *103*, 5440.

(22) Hager, J.; Wallace, S. C. *Journal of Physical Chemistry* **1984**, *88*, 5513.

(23) Henson, B. F.; Hartland, G. V.; Venturo, V. A.; Felker, P. M. *Journal of Chemical Physics* **1992**, *97*, 2189.

(24) Tsuzuki, S.; Honda, K.; Uchimaru, T.; Mikami, M.; Tanabe, K. *Journal of Physical Chemistry A* **1999**, *103*, 8265.

(25) Oki, M.; Iwamura, H. *Bulletin of the Chemical Society of Japan* **1959**, *32*, 955.

(26) Oki, M.; Iwamura, H.; Onoda, T.; Iwamura, M. *Tetrahedron* **1968**, *24*, 1905.

(27) Perutz, M. F.; Fermi, G.; Abraham, D. J.; Poyart, C.; Bursaux, E. *Journal of the American Chemical Society* **1986**, *108*, 1064.

(28) Rodham, D.A.; Suzuki, S.; Suenram, R.D.; Lovas, F.J.; Dasgupta, S.; Goddard, W.A. ; Blake, G.A., *Nature*, **1993**, 362, 735.

(29) Ottiger, P.; Pfaffen, C.; Leist, R.; Leutwyler, S.; Bachorz, R. A.; Klopper, W. *Journal of Physical Chemistry B* **2009**, *113*, 2937.

(30) Biswal, H.S.; Wategaonkar, S., *The Journal of Physical Chemistry A*, **2009**, 113, 12774.

(31) Mishra, B. K.; Arey, J. S.; Sathyamurthy, N. *Journal of Physical Chemistry A* **2010**, *114*, 9606.

(32) Guin, M.; Patwari, G. N.; Karthikeyan, S.; Kim, K. S. *Physical Chemistry Chemical Physics* **2009**, *11*, 11207.

(33) Felker, P. M. *J. Phys. Chem.* **1992**, *96*, 7844.

(34) Ebata, T.; Watanabe, T.; Mikami, N. *J. Phys. Chem.* **1995**, *99*, 5761.

(35) Weichert, A.; Reihn, C.; Brutschy, B. *J. Phys. Chem. A* **2001**, *105*, 5679.

(36) Hobza, P.; Riehn, C.; Weichert, A.; Brutschy, B. *Chem. Phys.* **2002**, *283*, 331.

(37) Kolaski, M.; Kumar, A.; Singh, N. J.; Kim, K. S. *Phys. Chem. Chem. Phys.* **2010**, *12*,

6278.

(38) Boys, S. F.; Bernadi, F. *Mol. Phys.* **1970**, *19*, 553.

(39) Frisch, M. J.; Trucks, G. W.; Schlegel, H. B.; et al. *GAUSSIAN 03*, Revision E.01, Gaussian, Inc., Wallingford, CT, 2004.

(40) Bylaska, E. J.; de Jong, W. A.; Govind, N.; et al. *NWChem, A Computational Chemistry Package for Parallel Computers,* Version 5.1.1 (2008), Pacific Northwest National Laboratory, Richland, Washington, USA.

(41) Carney, J.R., Zwier, T.S., *The Journal of Physical Chemistry A*, **1999**, 103, 9943.

(42) Carney, J.R.; Hagemeister, F.C.; Zwier, T.S., *J. Chem. Phys.*, **1998**, 108, 3379.

(43) Unterberg, C.; Jansen, A.; Gerhards, M., *J. Chem. Phys.*, **2000**, 113, 7945.

(44) Zhao, Y.; Truhlar, D. G. *Acc. Chem. Res.* **2008**, *41*, 157.

(45) Kumar, S.; Biswas, P.; Kaul, I.; Das, A., *Journal of Physical Chemistry A* ,**2011**(submitted).

(46) Sakota, K.; Shimazaki, Y.; Sekiya, H.; *J. Chem. Phys.*, **2009**, 130, 231105.